



“BABEȘ-BOLYAI” UNIVERSITY

Faculty of Physics

Ph.D Thesis Summary

**The effects of silver codoping on glass systems as
 $\text{Bi}_2\text{O}_3\cdot\text{PbO}$ and $\text{TeO}_2\cdot\text{PbO}$ doped with Gd^{3+} and Nd^{3+}
ions**

Tothăzan (Păs) Niculina-Amalia

Scientific supervisor:

Prof. Dr. Culea Eugen

Cluj-Napoca

-2019-

Table of content

I. INTRODUCTION	3
1.1. General considerations on vitreous materials	3
1.2. Glass materials based on bismuth, lead and tellurium.....	4
1.2.1. Bismuth oxide	4
1.2.2. Lead oxide	5
1.2.3. The binary vitreous system $x\text{Bi}_2\text{O}_3 \cdot y\text{PbO}$	6
1.2.4. Tellurium oxide	7
1.2.5. The binary vitreous system $\text{TeO}_2 \cdot \text{PbO}$	10
1.3. The effects of doping with rare earth ions as Gd^{3+} and Nd^{3+} on vitreous materials.....	11
1.4. The effects of co-doping with Ag^+ ions.....	13
REFERENCES.....	14
II. RESEARCH METHODOLOGY AND MATERIAL BASE	17
2.1. Obtaining oxide glasses.....	17
2.1.1. Melt undercooling method	17
2.2. Study methods of oxide glasses	18
2.2.1. X-ray diffraction	18
2.2.2. Infrared absorption spectroscopy (IR)	23
2.2.3. Density measurements	25
2.2.4. Magnetic susceptibility	26
2.2.5. UV-vis spectroscopy	29
2.2.6. Luminescence	32
REFERENCES.....	34
III. SAMPLE PREPARATION. RESEARCH TECHNIQUES USED	35
3.1. Preparation and processing of the sample	35
3.1.1. Preparation of $(100-x-y)[\text{Bi}_2\text{O}_3 \cdot \text{PbO}] \cdot x\text{Gd}_2\text{O}_3 \cdot y\text{Ag}_2\text{O}$ system	35
3.1.2. Preparation of $(100-x)[80\text{TeO}_2 \cdot 20\text{PbO}] \cdot 0.5\text{Ag}_2\text{O} \cdot x\text{Gd}_2\text{O}_3$ and $(100-x)[80\text{TeO}_2 \cdot 20\text{PbO}] \cdot 0.3\text{AgNPs} \cdot x\text{Gd}_2\text{O}_3$ systems	36
3.1.3. Preparation of $80\text{TeO}_2 \cdot (19,7-x)\text{PbO} \cdot 0,3\text{AgNPs} \cdot x\text{Nd}_2\text{O}_3$ and $80\text{TeO}_2 \cdot (19,85-x)\text{PbO} \cdot 0,15\text{Ag}_2\text{O} \cdot x\text{Nd}_2\text{O}_3$ systems	37
3.2. Research techniques used	38
3.2.1. X-ray diffraction	38

3.2.2. Infrared absorption spectroscopy (IR)	39
3.2.3. Magnetic susceptibility	41
3.2.4. Density measurements	45
3.2.5. UV-vis spectroscopy	46
3.2.6. Luminescence	49
REFERENCES.....	53
IV. THE STUDY ON [Bi₂O₃·PbO] AND [80TeO₂·20PbO] SYSTEMS	54
4.1. The study by X-ray diffraction	54
4.1.1. (100-x-y)[Bi ₂ O ₃ ·PbO]·xGd ₂ O ₃ ·yAg ₂ O	54
4.1.2. (100-x)[80TeO ₂ ·20PbO]·0,5Ag ₂ O·xGd ₂ O ₃ and (100-x)[80TeO ₂ ·20PbO]·0,3AgNPs·xGd ₂ O ₃	56
4.1.3. 80TeO ₂ ·(19,7-x)PbO·0,3AgNPs·xNd ₂ O ₃ and 80TeO ₂ ·(19,85-x)PbO·0,15Ag ₂ O·xNd ₂ O ₃	59
4.2. The study of infrared absorption spectroscopy (IR).....	62
4.2.1. (100-x-y)[Bi ₂ O ₃ ·PbO]·xGd ₂ O ₃ ·yAg ₂ O	62
4.2.2. (100-x)[80TeO ₂ ·20PbO]·0,5Ag ₂ O·xGd ₂ O ₃ and (100-x)·[80TeO ₂ ·20PbO]·0,3AgNPs·xGd ₂ O ₃	65
4.3. Magnetic susceptibility measurements	69
4.3.1. (100-x-y)[Bi ₂ O ₃ ·PbO]·xGd ₂ O ₃ ·yAg ₂ O	69
4.3.2. (100-x)[80TeO ₂ ·20PbO]·0,5Ag ₂ O·xGd ₂ O ₃ and (100-x) [80TeO ₂ ·20PbO]·0,3AgNPs·xGd ₂ O ₃	70
4.3.3. 80TeO ₂ ·(19,7-x)PbO·xNd ₂ O ₃ ·0,3AgNPs and 80TeO ₂ ·(19,85-x)PbO·xNd ₂ O ₃ ·0,15Ag ₂ O	74
4.4. Density measurements	77
4.4.1. (100-x-y)[Bi ₂ O ₃ ·PbO]·xGd ₂ O ₃ ·yAg ₂ O	77
4.4.2. (100-x)[80TeO ₂ ·20PbO]·0,5Ag ₂ O·xGd ₂ O ₃ and (100-x)[80TeO ₂ ·20PbO]·0,3AgNPs·xGd ₂ O ₃	78
4.4.3. 80TeO ₂ ·(19,7-x)PbO·0,3AgNPs·xNd ₂ O ₃ and 80TeO ₂ ·(19,85-x)PbO·0,15Ag ₂ O·xNd ₂ O ₃	79
4.5. The study by UV-Vis spectroscopy.....	81
4.5.1. 80TeO ₂ ·(19,7-x)PbO·xNd ₂ O ₃ ·0,3AgNPs and 80TeO ₂ ·(19,85-x)PbO·xNd ₂ O ₃ ·0,15Ag ₂ O	81
4.6. The study by luminescence	85
4.6.1. 80TeO ₂ ·(19,7-x)PbO·xNd ₂ O ₃ ·0,3AgNPs and 80TeO ₂ ·(19,85-x)PbO·xNd ₂ O ₃ ·0,15Ag ₂ O	85
REFERENCES.....	89
V. CONCLUSIONS	92
ACKNOWLEDGMENT	98

KEYWORDS: rare earth oxides, co-doping, X-ray diffraction, density, infrared spectroscopy, magnetic susceptibility, UV-Vis, luminescence.

I. INTRODUCTION

1.1. General considerations on vitreous materials

The non-crystalline solid state occupies an important place in the research of condensed matter physics. This is due to a multitude of scientific and applicative reasons. Thus, on the one hand, the information obtained by studying the vitreous materials allowed to clarify important aspects from a scientific point of view. On the other hand, the acquired knowledge has been useful in technological, applicative achievements [1, 2].

At the moment, there is a particular interest for glass and glass-ceramic materials with potential for applicability in the field of telecommunications (lasers, sensors, signal amplifiers, optical fibers, etc.) and electronics. These materials must have certain optical qualities, chemical stability and mechanical resistance. For this reason it is very important to know if the material is stable in the vitreous state or tends to crystallize, respectively it is important to identify any crystallization phenomena that may occur during the preparation process [3,4].

Heavy metal glasses, such as bismuth and telluride, have important properties such as high refractive index (> 2.0), optical non-linearity and good transmission over large areas (from UV-Vis to IR). which make them extremely interesting for applications in telecommunications, respectively those related to the field of photonics and optoelectronics [1, 2, 5].

Co-doping of rare earth ion (RE) doped glass and glass ceramic with a second species of RE ions or with noble metal nanoparticles can produce extremely interesting structural and behavioral effects (eg, the phenomenon of converting IR radiation to visible or a significant amplification of the radiation emission), important for various applications [6, 7]. In this regard, we emphasize that although the telltale materials have been recognized as important for

telecommunications and photonics, there is relatively little information related to the structural and behavioral changes that are caused by the incorporation of noble metal nanoparticles [8]. An interesting but controversial aspect at the same time is related to the co-doping of RE - noble metal which, in some situations, produces an amplification of the emission of RE ions, an effect attributed to the resonance of surface plasmas or to energy transfers between very small (molecular) ion aggregates. of noble metal and RE ions [9]

1.4. The effects of co-doping with Ag⁺ ions

The glasses containing silver are of great interest due to their stability, their resistance to humidity and their high electrical conductivity in the range 10^0 and $10^{-2}\Omega\text{m}^{-1}$, at room temperature [59,60].

As it's known, the solubility of Ag₂O is limited in glasses by certain thermodynamic factors, by the partial pressure of oxygen, by the temperature and by the composition of the glass. The glasses with the Bi₂O₃-PbO-Ag₂O matrix, based on the oxides of two heavy metals as lattice formers (Bi₂O₃ and PbO) and containing a large amount of Ag₂O (up to 30 mol%), were obtained using the ultra-fast subtraction method. of the melt with the help of twin-roller equipment. These glasses have very good ionic conductivity, important for applications of solid state electrochemical devices [59].

The glasses containing silver also attracted attention because of their antibacterial activity. Thus, it is known that the Ag ion prevents the growth of the bacterial population [61, 62].

The structural changes produced by heat treatment on the bismuth-lead-silver systems doped with erbium have been observed by X-ray diffraction and FTIR spectroscopy studies. The heat treatment applied to the samples produces the crystallization of these glasses, the presence of the crystalline phases Bi₂O₃ and PbO_{1.44} being highlighted by X-ray diffraction analysis.

FTIR data suggest the presence of both the BiO₆ and BiO₃ structural units, as well as those of the PbO₄ and PbO₃ type in the studied bismuth-lead-silver glasses. The amount of structural units BiO₃ and PbO₄ is higher in the heat treated samples [63].

II. RESEARCH METHODOLOGY AND MATERIAL BASE

2.1. Obtaining oxide glasses

2.1.1. Melt undercooling method

The method of melt undercooling is based on the idea of "freezing" the melt so that, in general, the disordered structure existing in the melt (in liquid state) is preserved in the solid state [1]. For this, a rapid cooling of the melts under the solidification temperature is achieved, avoiding the occurrence of the nucleation process, respectively of the crystallization process.

For the preparation of a glass by the method of undercooling the melts, a mixture of raw materials according to the desired chemical composition is obtained first, the mixture is melted by keeping it in the oven for a fixed duration, at a well-established temperature (above the melting temperature), after which produces rapid cooling of the melt by pouring it on a stainless steel plate, generally at room temperature. The melting must be cooled sufficiently quickly to prevent nucleation and thus partial crystallization of the glass. In general, it is intended that by cooling to obtain a solid glass having the melt structure from which it is obtained.

We mention that the cooling method used must provide the cooling rate required to obtain the vitreous state.

2.2. Study methods of oxide glasses

The study of oxide glasses with rare earth ions aims to gather information on their structure and properties, in order to find new practical uses. The study methods used in this work are: X-ray diffraction, infrared spectroscopy (FT-IR), density measurements, magnetic susceptibility and luminescence measurements.

III. SAMPLES PREPARATION. RESEARCH TECHNIQUES USED

3.1. Preparation and processing of the sample

In order to carry out a study on the influence of co-doping with silver ions or silver nanoparticles of oxide glasses doped with rare earth ions, a few new glass systems have been prepared.

We mention that these glass systems are new, original, were prepared and investigated for the first time in the present study and have not been previously reported in the literature.

In these systems it is possible for rare earth ions to be arranged both in the positions corresponding to the vitreous lattice modifier and to those of the vitreous lattice modifier [1-3]. This arrangement of rare earth ions allows homogeneous glasses to be obtained up to high concentrations of paramagnetic ions.

Samples were prepared by melt undercooling method.

The sample composition of the studied system $(100-x-y)[\text{Bi}_2\text{O}_3\cdot\text{PbO}]\cdot x\text{Gd}_2\text{O}_3\cdot y\text{Ag}_2\text{O}$ is presented in the table below.

Table 3.1 Composition of samples from the system $(100-x-y)[\text{Bi}_2\text{O}_3\cdot\text{PbO}]\cdot x\text{Gd}_2\text{O}_3\cdot y\text{Ag}_2\text{O}$

Sample no.	Bi₂O₃ [mol%]	PbO [mol%]	Gd₂O₃ [mol%]	Ag₂O [mol%]
1	50	50	-	-
2	49.75	49.75	-	0.5
3	49.25	49.25	1	0.5
4	47.25	47.25	5	0.5
5	49.50	49.50	1	-
6	47.50	47.50	5	-

The table below shows the composition of the samples prepared from the $(100-x)[80\text{TeO}_2\cdot 20\text{PbO}]\cdot 0.5\text{Ag}_2\text{O}\cdot x\text{Gd}_2\text{O}_3$ systems noted S_x ($x = 1-5$) and $(100-x)[80\text{TeO}_2\cdot 20\text{PbO}]\cdot 0.3\text{AgNPs}\cdot x\text{Gd}_2\text{O}_3$ noted S_x' ($x = 1-5$).

Table 3.2. Composition of samples prepared from $(100-x)[80\text{TeO}_2\cdot 20\text{PbO}]\cdot 0.5\text{Ag}_2\text{O}\cdot x\text{Gd}_2\text{O}_3$ rated S_x ($x = 1-5$) and $(100-x)[80\text{TeO}_2\cdot 20\text{PbO}]\cdot 0.3\text{AgNPs}\cdot x\text{Gd}_2\text{O}_3$ rated S_x' ($x = 1-5$).

Sample no.	80TeO ₂ ·20PbO [mol%]	Ag ₂ O [mol%]	AgNP [mol%]	Gd ₂ O ₃ [mol%]
S0	100	-	-	-
S1	99.50	0.50	-	-
S1'	99.70	-	0.30	-
S2	98.50	0.50	-	1
S2'	98.70	-	0.30	1
S3	96.50	0.50	-	3
S3'	96.70	-	0.30	3
S4	94.50	0.50	-	5
S4'	94.70	-	0.30	5
S5	89.50	0.50	-	10
S5'	89.70	-	0.30	10

Two vitroc ceramic systems 80TeO₂·(19.7-x) PbO·0.3AgNPs·xNd₂O₃ noted further S_x (x=1-5) and 80TeO₂·(19.85-x) PbO·0.15Ag₂O·xNd₂O₃ noted S_x' (x=1-5) with the chemical composition shown in table 3.3.

Table 3.3. Concentrations of the components of 80TeO₂ systems (19.7-x) PbO·0.3AgNPs·xNd₂O₃ noted further S_x (x=1-5) and 80TeO₂·(19.85-x) PbO·0.15Ag₂O · xNd₂O₃ noted S_x' (x = 1-5).

Sample no.	Composition [mol%]				
	TeO ₂	PbO	Ag ₂ O	AgNPs	Nd ₂ O ₃
S0	80	20	0	-	0
S1	80	19.70	-	0.3	0
S1'	80	19.85	0.15	-	0
S2	80	18.70	-	0.3	1
S2'	80	18.85	0.15		1
S3	80	16.70	-	0.3	3
S3'	80	16.85	0.15	-	3
S4	80	14.70	-	0.3	5
S4'	80	14.85	0.15	-	5
S5	80	9.70	-	0.3	10
S5'	80	9.85	0.15		10

IV. THE STUDY ON $[\text{Bi}_2\text{O}_3 \cdot \text{PbO}]$ AND $[\text{80TeO}_2 \cdot \text{20PbO}]$ SYSTEMS

4.1. The study by X-ray diffraction

4.1.1. $(100-x-y)[\text{Bi}_2\text{O}_3 \cdot \text{PbO}] \cdot x\text{Gd}_2\text{O}_3 \cdot y\text{Ag}_2\text{O}$

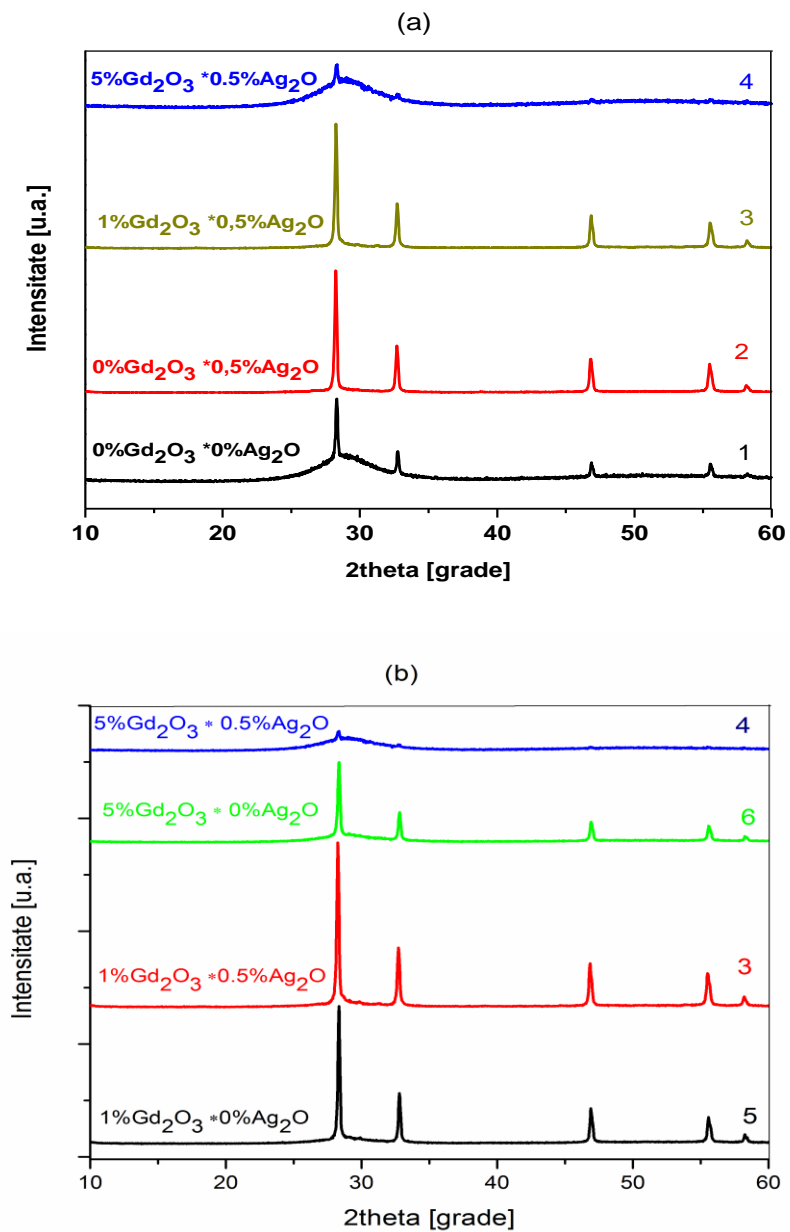


Fig.4.1. X-ray diffraction pattern for $(100-x-y)[\text{Bi}_2\text{O}_3 \cdot \text{PbO}] \cdot x\text{Gd}_2\text{O}_3 \cdot y\text{Ag}_2\text{O}$ system

In figure 4.1.a it can be observed that for samples 1 - 3 the diffractions pattern obtained are characteristic of the glass ceramic structures. Here, together with the amorphous phase, diffraction peaks corresponding to crystalline phases appear. These peaks decrease in intensity with increasing Gd_2O_3 content in samples so that for sample 4 they almost disappear [2]. The obtained spectra were analyzed with the help of a specialized program that revealed the presence of several crystalline phases in the samples, namely δBi_2O_3 cubic FC, $PbO_{1.44}$ simple cubic, as well as traces of $Bi_{1.208}Gd_{0.792}O_3$ cubic FC with lattice parameters very close [3].

It is noted that the samples are sensitive to the Gd_2O_3 content. Thus, increasing the Gd_2O_3 content reduces the crystallization process of the samples in intensity.

4.1.2. $(100-x)[80TeO_2 \cdot 20PbO] \cdot 0,5Ag_2O \cdot xGd_2O_3$ and $(100-x)[80TeO_2 \cdot 20PbO] \cdot 0,3AgNPs \cdot xGd_2O_3$

4.2 figure present x-ray diffraction pattern for $(100-x)[80TeO_2 \cdot 20PbO] \cdot 0,5Ag_2O \cdot xGd_2O_3$ and $(100-x)[80TeO_2 \cdot 20PbO] \cdot 0,3AgNPs \cdot xGd_2O_3$ systems.

It can be seen from the figure that the samples contain both crystalline and amorphous phase. Samples without Gd_2O_3 are amorphous. After addition of Gd_2O_3 to the samples, crystalline phases also appear, their amount increasing proportionally with the increase of gadolinium ion concentration in the samples. Thus, the crystalline phases appear in sample S1' and their concentration increases in samples S2, S2', S3, the maximum appearing in sample S3'.

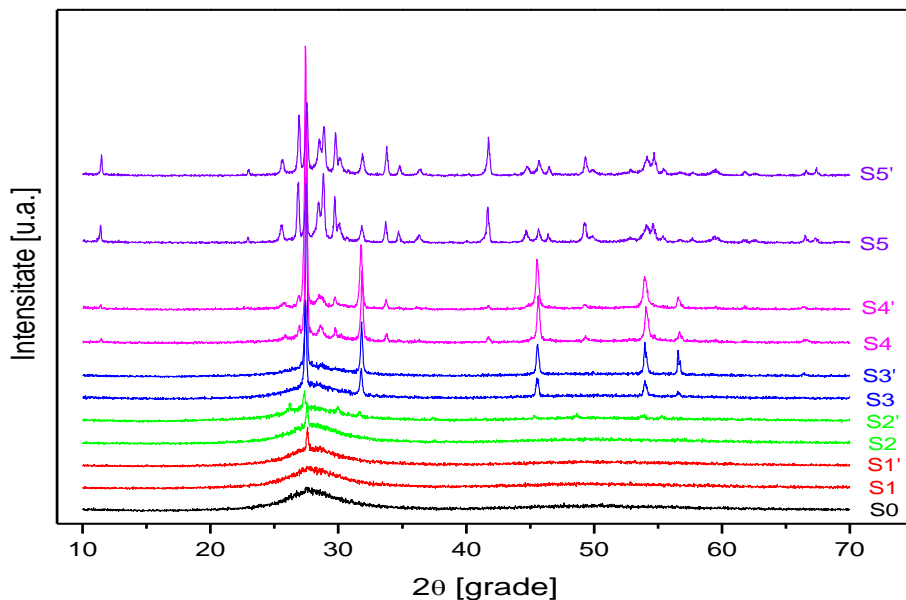


Fig.4.2. X-ray diffraction pattern for $(100-x)[80\text{TeO}_2 \cdot 20\text{PbO}] \cdot 0,5\text{Ag}_2\text{O} \cdot x\text{Gd}_2\text{O}_3$ and $(100-x)[80\text{TeO}_2 \cdot 20\text{PbO}] \cdot 0,3\text{AgNPs} \cdot x\text{Gd}_2\text{O}_3$ systems

The crystalline phases highlighted by X-ray diffractograms were identified as $\text{Gd}_2\text{Te}_6\text{O}_{15}$ and $\text{Pb}_2\text{Te}_3\text{O}_7$. The two crystalline phases belong to the cubic system with centered faces, $\text{Gd}_2\text{Te}_6\text{O}_{15}$ having the lattice parameter $a = 5.611 \text{ \AA}$ and $\text{Pb}_2\text{Te}_3\text{O}_7$ having $a = 5.647 \text{ \AA}$. The increase of the crystalline phase with the concentration of Gd_2O_3 highlights the important role of gadolinium in the crystallization process.

In the amorphous host matrix, after the addition of Gd_2O_3 , the crystalline phases $\text{Pb}_2\text{Te}_3\text{O}_7$ and $\text{Gd}_2\text{Te}_6\text{O}_{15}$ develop. Using the Debye-Scherrer formula [4, 5] we evaluated the size of the crystallites. For this the width at half of the maximum diffraction peak was taken into account. For samples S0, S1 and S1' these dimensions were approximately 20 \AA , which means 3×3.3 structural units in a crystallite.

An additional crystalline phase, namely $\text{Gd}_2\text{Te}_4\text{O}_{11}$, appears in samples S4 and S4', which increases in concentration for samples S5 and S5'. This phase, which crystallizes in the monoclinic system, is iso-structural with $\text{Sm}_2\text{Te}_4\text{O}_{15}$ and $\text{Tb}_2\text{Te}_4\text{O}_{11}$. Samples S5 and S5' contain a small amount of different polymorphs corresponding to the crystalline phases of PbO and PbO_2 .

Figure 4.3 shows only the most intense diffractions of these polymorphs.

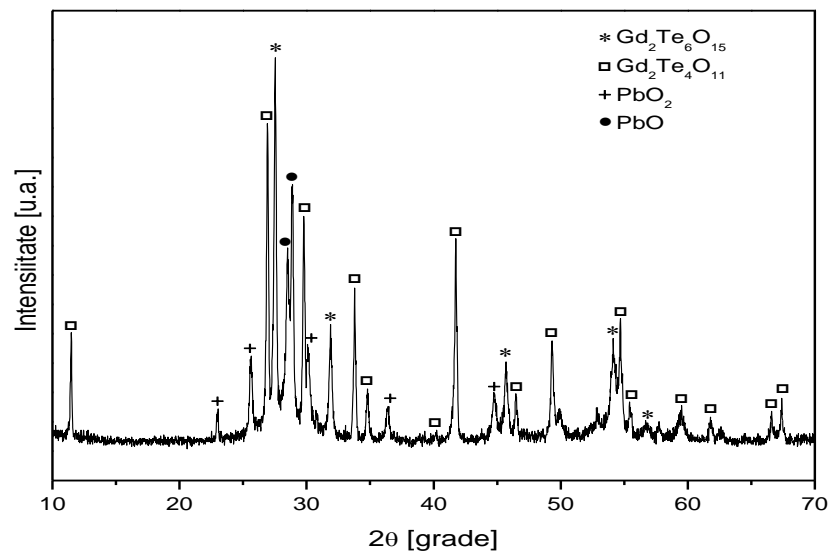


Fig.4.3. The crystalline phases of sample S5'

The average size of the cubic crystalline phase grains, D , was calculated using the Debye-Scherrer formula [4, 5]. The degree of crystallinity, X_c , was estimated as a ratio of the surface of the diffraction peaks and of the total diffraction surface (which includes diffraction peaks and amorphous halos) using the Reflex software, contained in the Material Studio software package [6].

Figure 4.4 shows the compositional evolution of D in figure 4.4a, and X_c in figure 4.4b. The lines are drawn as a visual guide.

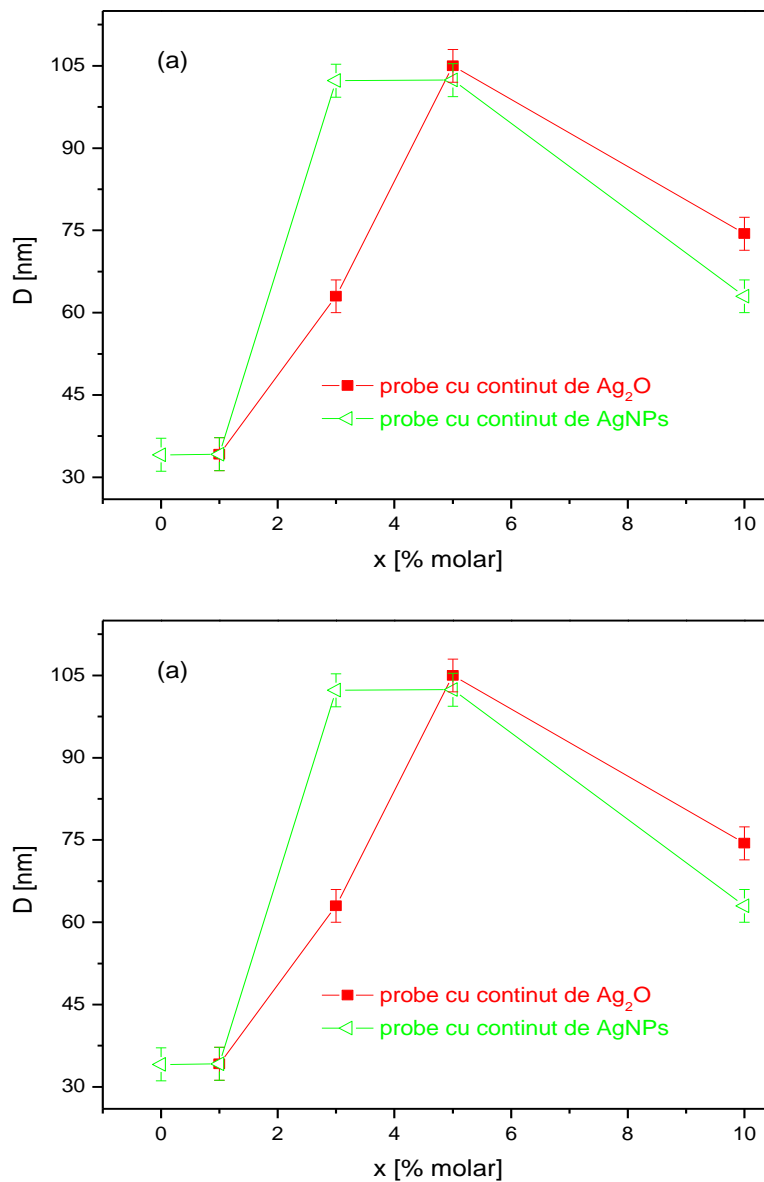
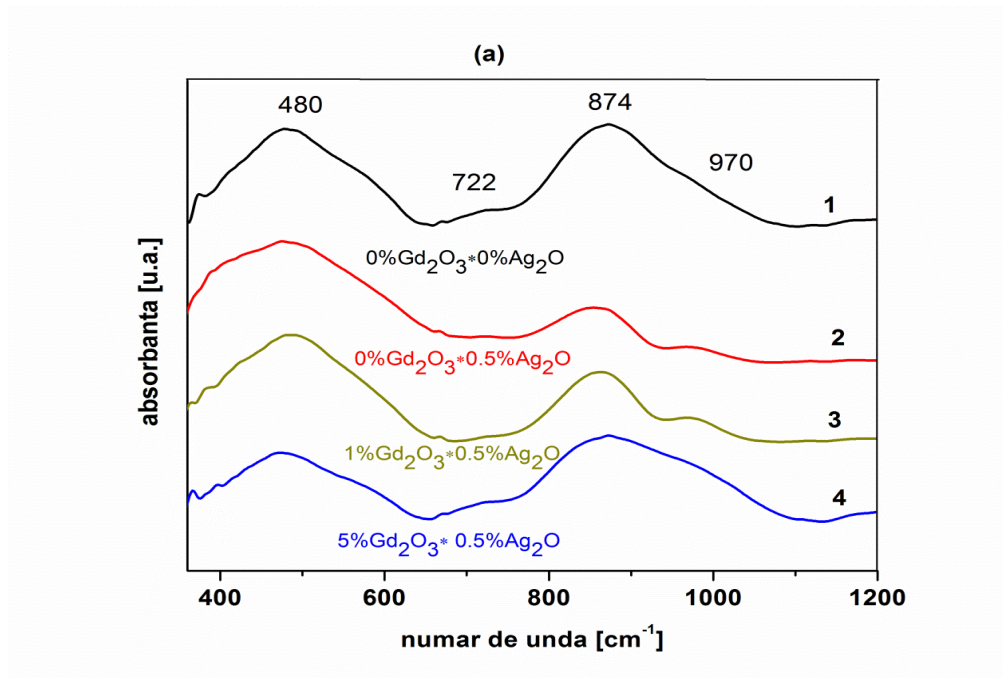


Fig. 4.4. The compositional dependence of the average size of the crystallite (a) and the degree of crystallinity (b) for the studied samples.

The size of crystallite D increases with increasing the Gd_2O_3 content up to $x = 5$ mol%, and decreases slightly for samples S5 and S5' with the formation of the $Gd_2Te_4O_{11}$ phase. The degree of crystallinity X_c increases with the Gd_2O_3 content for both series of samples (codoped with Ag_2O , respectively AgNPs) throughout the composition range. It should be noted that the X_c values for the samples codoped with AgNPs are higher than the samples codoped with silver ions. This behavior is due to the fact that when co-doping with AgNPs they are embedded in the host matrix whereas when co-doping with Ag_2O the ions of Ag are inserted into the host matrix as lattice modifiers [7].

4.2. The study of infrared absorption spectroscopy (IR)

4.2.1. $(100-x-y)[Bi_2O_3 \cdot PbO] \cdot xGd_2O_3 \cdot yAg_2O$



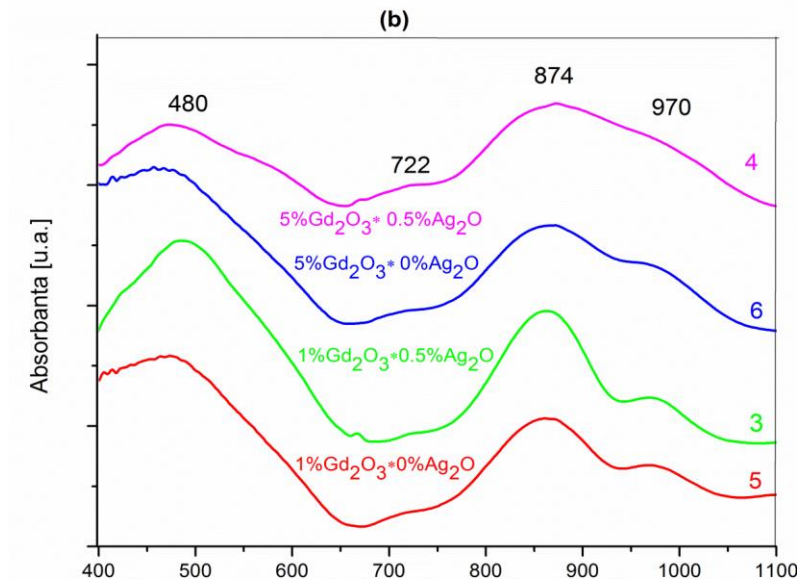


Fig.4.6. The FTIR absorption spectra of the system $(100-x-y)[\text{Bi}_2\text{O}_3\cdot\text{PbO}]\cdot x\text{Gd}_2\text{O}_3\cdot y\text{Ag}_2\text{O}$

Table 4.2. Assignment of absorption bands in the IR spectrum of the system $(100-x-y)[\text{Bi}_2\text{O}_3\cdot\text{PbO}]\cdot x\text{Gd}_2\text{O}_3\cdot y\text{Ag}_2\text{O}$

Wave number (cm-1)	Assignment of absorption bands in the IR spectrum
480	Bi-O bending vibration in BiO_6 and/or BiO_3 [3,12] Pb-O bonds vibration [3,12]
722	Pb-O bonds vibration in PbO_n , where $n = 3$ and/or 4 [3,12]
874	Bi-O symmetrical stretching vibration in BiO_6 polyhedron [3,12]
970	Pb-O symmetrical stretching vibration in different structural units [3,12]

4.2.2. $(100-x)[80\text{TeO}_2\cdot 20\text{PbO}]\cdot 0,5\text{Ag}_2\text{O}\cdot x\text{Gd}_2\text{O}_3$ and $(100-x)\cdot [80\text{TeO}_2\cdot 20\text{PbO}]\cdot 0,3\text{AgNPs}\cdot x\text{Gd}_2\text{O}_3$

FTIR spectra of lead vitroceraamics doped with gadolinium ions and co-doped with fixed amounts of silver oxide (Ag_2O) or silver nanoparticles (AgNPs) were used to investigate the local structure of the samples.

Figure 4.8 shows the IR absorption spectra of leaded glass glasses and vitroceraamics from $(100-x)[80\text{TeO}_2\cdot 20\text{PbO}]\cdot 0,5\text{Ag}_2\text{O}\cdot x\text{Gd}_2\text{O}_3$ and $(100-x)\cdot [80\text{TeO}_2\cdot 20\text{PbO}]\cdot 0,3\text{AgNPs}\cdot x\text{Gd}_2\text{O}_3$.

The deconvolution of the experimental FTIR bands was necessary, since most of them are large, representing an envelope of several superimposed absorption bands.

Figure 4.9 shows as representative examples the cases of deconvolution in the Gaussian bands of the FTIR spectrum for samples S2 (fig. 4.9 a) and S5' (fig. 4.9 b).

The IR strips thus obtained were then assigned (Table 4.2.) based on the data available in the specialty literature for vitreous and vitroceramic leaded systems [8,16].

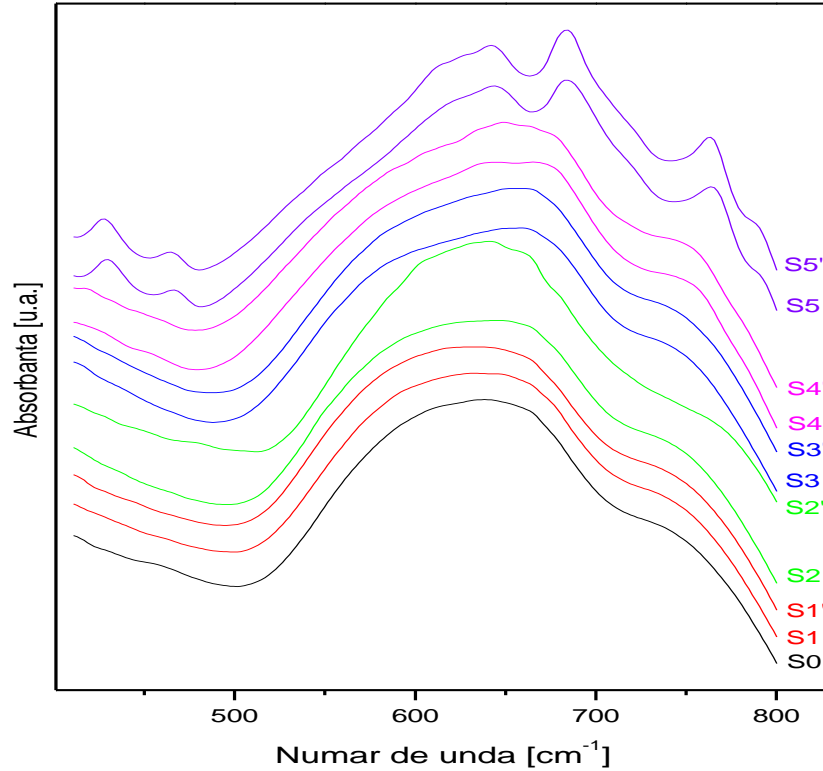


Fig.4.8. FTIR spectra of $(100-x)[80\text{TeO}_2 \cdot 20\text{PbO}] \cdot 0,5\text{Ag}_2\text{O} \cdot x\text{Gd}_2\text{O}_3$ and $(100-x) \cdot [80\text{TeO}_2 \cdot 20\text{PbO}] \cdot 0,3\text{AgNPs} \cdot x\text{Gd}_2\text{O}_3$ systems samples

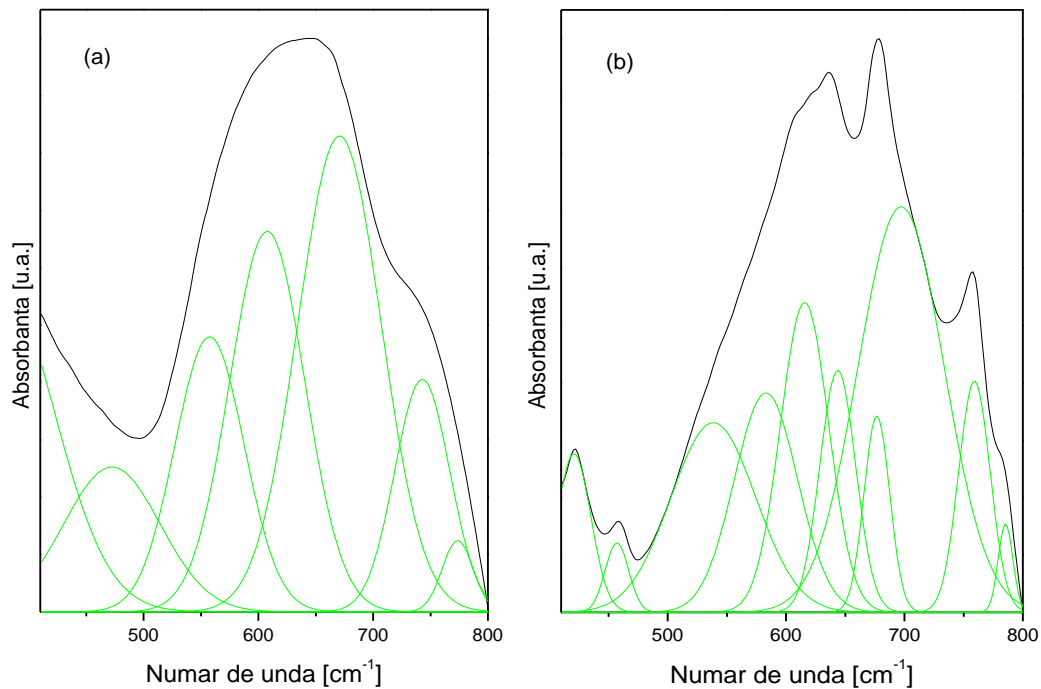


Fig.4.9. Deconvolution of the FTIR spectra for S2 (a) and S5' (b) samples

Table 4.3. Assignment of IR bands of $(100-x)[80\text{TeO}_2 \cdot 20\text{PbO}] \cdot 0,5\text{Ag}_2\text{O} \cdot x\text{Gd}_2\text{O}_3$ and $(100-x) \cdot [80\text{TeO}_2 \cdot 20\text{PbO}] \cdot 0,3\text{AgNPs} \cdot x\text{Gd}_2\text{O}_3$

Wave number [cm ⁻¹]	Assignment
362-488	Te-O-Te or O-Te-O bending vibration [6,8] Pb-O stretching vibrations in PbO ₄ units [6,8]
537-561	Pb-O symmetrical bending vibration [5,8] Ag-O bonds vibration [8]
583-617	Te-O stretching vibration in TeO ₄ units [4, 6, 17]
644-698	Te-O bonds vibration in TeO ₄ units [4, 8, 16] Pb-O vibration in PbO _n pyramidal units (n = 3 and/or 4) [4, 8, 16]
742-759	Te-O bonds vibration in TeO ₃ units [6]
773-786	Te-O ⁻ bonds vibration in TeO ₃ units [6]

As it results from the analysis of the data presented in this table, the FTIR spectra of the studied samples certify the presence of the structural units PbO_3 , PbO_4 , TeO_3 and TeO_4 in the studied samples.

To analyze the effect produced by the increase of gadolinium ion content and the influence of the codopant (Ag_2O or AgNPs), the ratio between the number of TeO_3 and TeO_4 structural units was calculated, where it was considered that this ratio is equal to the ratio of the sum of the integrated band intensities. IR absorption associated with the structural units TeO_3 , A_3 , respectively associated with the structural units TeO_4 , A_4 , ie $A_r = A_3 / A_4$.

The compositional evolution of the A_r parameter for both series of studied samples is shown in figure 4.10.

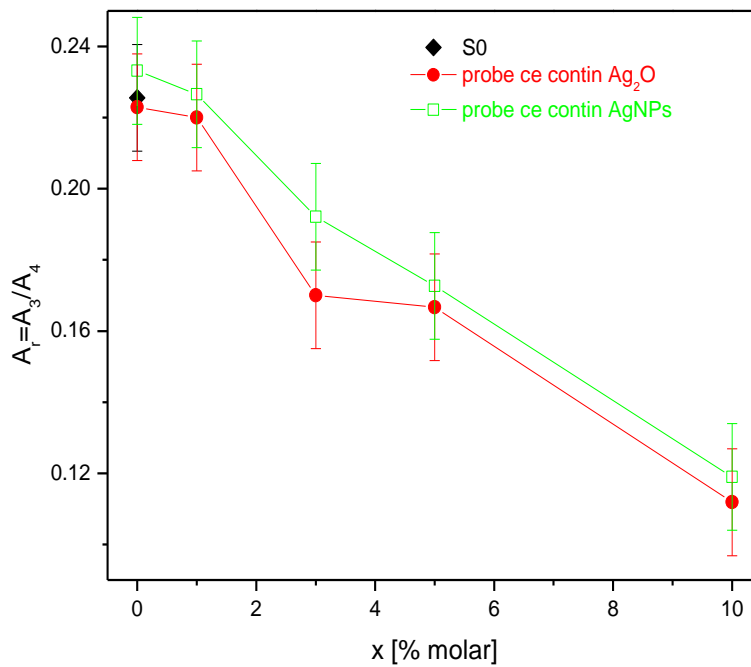


Fig.4.10. Dependence of the A_r ratio on the Gd_2O_3 content of the samples $(100-x)[80\text{TeO}_2 \cdot 20\text{PbO}] \cdot 0,5\text{Ag}_2\text{O} \cdot x\text{Gd}_2\text{O}_3$ and $(100-x) \cdot [80\text{TeO}_2 \cdot 20\text{PbO}] \cdot 0,3\text{AgNPs} \cdot x\text{Gd}_2\text{O}_3$.

For both series of samples, A_r decreases with increasing gadolinium content throughout the composition area. This evolution can be explained by the progressive conversion of the TeO_3 structural units into TeO_4 as the content of Gd_2O_3 increases. This assumption is also supported by X-ray diffraction data, being known that tellurium ions are present in the crystalline components usually in the 4+ valence state. For glass ceramic coated with silver metallic nanoparticles (AgNPs)

the Ar values are higher than for the samples coated with Ag₂O. This is related to the specific way in which the silver added under the two forms is inserted in the host matrix. Thus, if in the case of AgNPs it is a simple insertion into interstitial positions, in the case of Ag₂O codoping, silver ions are provided which are inserted into the structural chains of the host matrices, modifying their vibrational parameters.

These observations allow us to conclude that not only the content of gadolinium ions in the vitroceramics studied, but also the nature of the codopant (Ag₂O or AgNPs) plays an important role in defining the local structure of these samples.

4.3. Magnetic susceptibility measurements

4.3.1. (100-x-y)[Bi₂O₃·PbO]·xGd₂O₃·yAg₂O

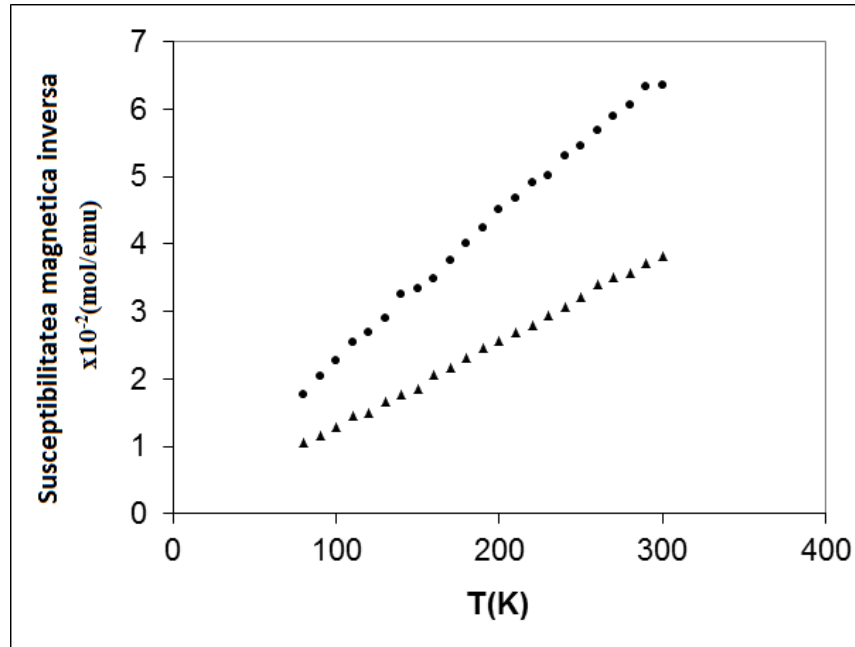


Fig.4.11. Dependence of the inverse temperature magnetic susceptibility- sample 3 (•) (x = 1 %mol) and sample 4 (▲) (x = 5 %mol)

The magnetic behavior of the samples is due to the presence of Gd³⁺ ions because for the host matrix Bi₂O₃ PbO a diamagnetic behavior was highlighted. The diamagnetic susceptibility of the vitreous matrix was measured (samples without Gd₂O₃), and this diamagnetic contribution was used to correct the experimental data obtained for the studied samples so as to show the effect of doping with gadolinium ions.

The values of the paramagnetic Curie temperature, θ_p , determined for the investigated samples are presented in table 4.4.

Table 4.4. The samples studied from the system $(100-x-y)[\text{Bi}_2\text{O}_3 \cdot \text{PbO}] \cdot x\text{Gd}_2\text{O}_3 \cdot y\text{Ag}_2\text{O}$ and their paramagnetic Curie temperature.

Sample no.	Bi₂O₃ [% mol]	PbO [% mol]	Gd₂O₃ [% mol]	Ag₂O [% mol]	θ_p [K]
3	49.25	49.25	1	0.5	-2
4	47.25	47.25	5	0.5	-5
5	49.50	49.50	1	-	-3
6	47.50	47.50	5	-	-4

Curie paramagnetic temperature is a primary indicator of the magnetic interactions that take place between Gd^{3+} magnetic ions. The θ_p values obtained and presented in the table are small and negative. This suggests that in our samples the Gd^{3+} ions appear predominantly as isolated species and in small number as species coupled through weak antiferromagnetic interactions.

4.4. Density measurements

4.4.1. $(100-x-y)[\text{Bi}_2\text{O}_3 \cdot \text{PbO}] \cdot x\text{Gd}_2\text{O}_3 \cdot y\text{Ag}_2\text{O}$

For all the samples studied in this paper, the density was determined using the pycnometer method. For this purpose the mass of the samples was measured using an analytical balance of five decimal using as the immersion liquid toluene with density 0.8669 g / cm^3 at 20°C . The density determination is based on Archimedes' law with the use of the formula:

$$\rho = \frac{m_a \cdot \rho_t}{m_a \cdot m_t} \quad (6)$$

where m_a is the mass of the sample in air, m_t is the mass of the sample in toluene and ρ_t is the density of toluene at working temperature.

The figure below shows the compositional density dependence for the bismuthed lead samples studied in the system $(100-x-y)[\text{Bi}_2\text{O}_3 \cdot \text{PbO}] \cdot x\text{Gd}_2\text{O}_3 \cdot y\text{Ag}_2\text{O}$. The lines joining the experimental points have the role of visual guide.

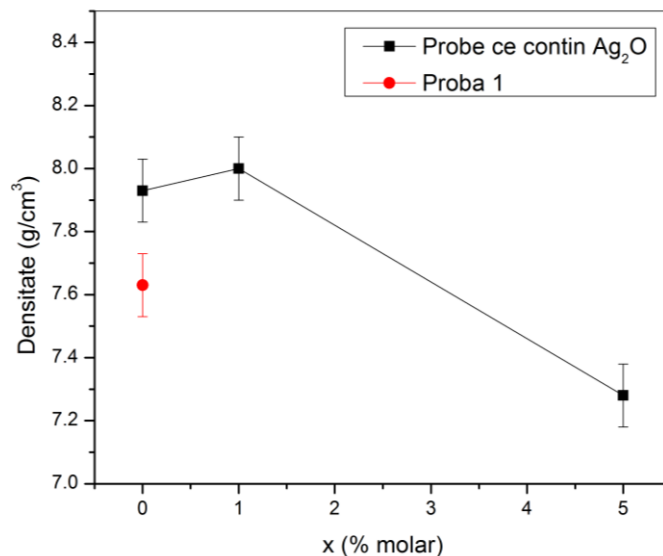


Fig. 4.15. Compositional density dependence for system samples $(100-x-y)[\text{Bi}_2\text{O}_3 \cdot \text{PbO}] \cdot x\text{Gd}_2\text{O}_3 \cdot y\text{Ag}_2\text{O}$

This compositional evolution of density can be explained by the fact that, as FTIR spectroscopy data show, the addition of Gd^{3+} ions results in the conversion of structural groups BiO_3 into BiO_6 , which leads to a tighter (less compact) sample structure.

4.5. UV-Vis spectroscopy

4.5.1. $80\text{TeO}_2 \cdot (19,7-x)\text{PbO} \cdot x\text{Nd}_2\text{O}_3 \cdot 0,3\text{AgNPs}$ and $80\text{TeO}_2 \cdot (19,85-x)\text{PbO} \cdot x\text{Nd}_2\text{O}_3 \cdot 0,15\text{Ag}_2\text{O}$

UV-Vis measurements were performed at room temperature, in reflection, on the wavelength range 350-1000 nm.

For all UV-Vis absorption spectra, the Kubelka-Munk remission functions, $F(R)$, have been obtained, where the function $F(R)$ can be considered proportional to the radiation absorbed [28]. The samples that do not contain neodymium have no absorption peaks and are in agreement with the data in the literature [8, 10], which is why they are not shown in figure 4.18.

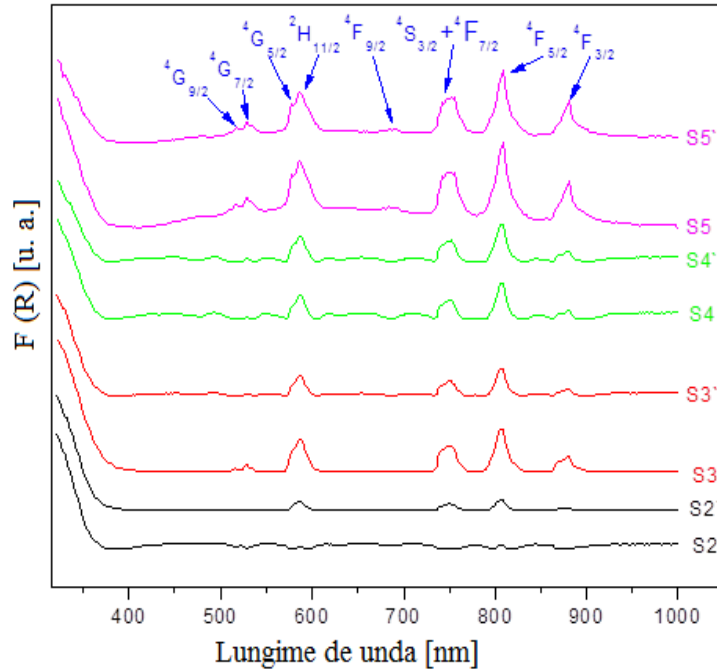


Fig. 4.18. UV-Vis spectra in reflection for the vitroceraamics studied

Eight peaks corresponding to the transitions from the fundamental level $^4I_{9/2}$ have been identified on various excited levels of Nd^{3+} ions, mentioned in figure 4.18. Thus these spectra confirm the existence of neodymium ions in the studied samples. Considering the previous results [29, 30], these peaks were assigned to transitions $^4I_{9/2} \rightarrow ^4G_{9/2}, ^4G_{7/2}, ^4G_{5/2}, 2H_{11/2}, ^4F_{9/2}, ^4S_{3/2} + ^4F_{7/2}, ^4F_{5/2}, ^4F_{3/2}$.

4.6. Luminescence

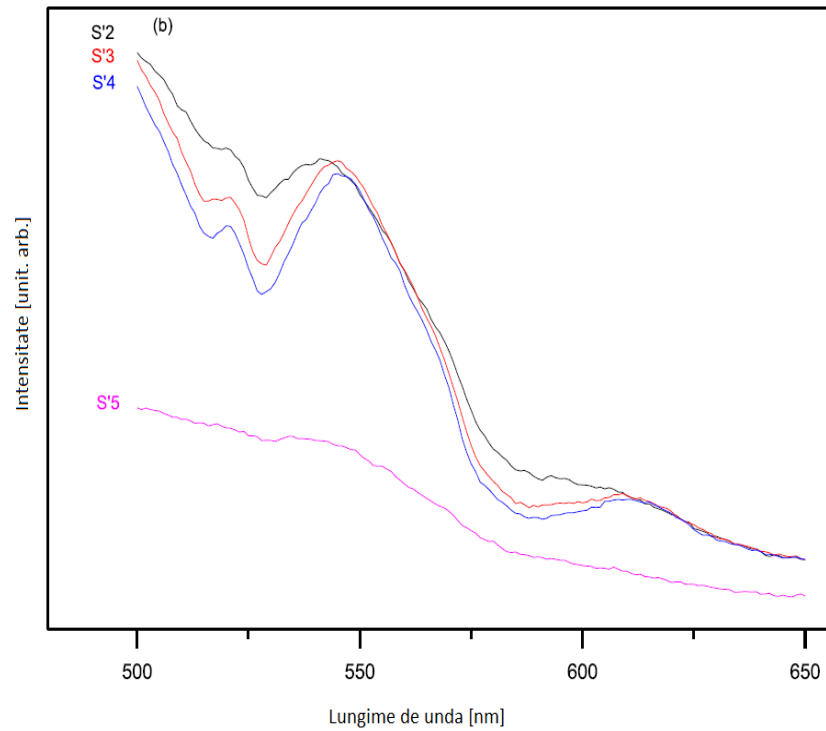
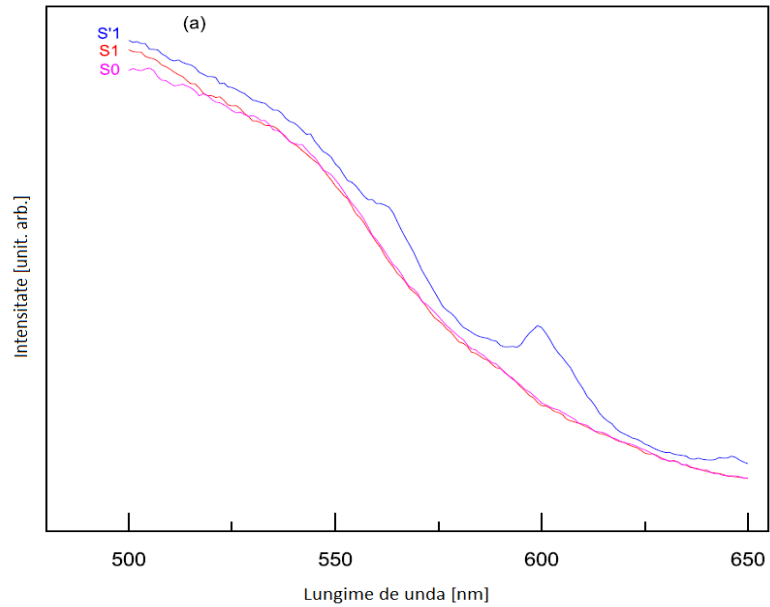
4.6.1. $80TeO_2 \cdot (19,7-x)PbO \cdot xNd_2O_3 \cdot 0,3AgNPs$ and $80TeO_2 \cdot (19,85-x)PbO \cdot xNd_2O_3 \cdot 0,15Ag_2O$

These spectra were obtained using excitation wavelength radiation of 808 nm. Excitation was performed at room temperature.

In figure 4.20a, the luminescence spectra of the neodymium-free samples can be observed, and in the figures 4.20b and 4.20c the luminescence spectra of the neodymium-doped samples and co-doped with AgNPs and Ag_2O .

Different behavior of samples S0, S1 and S1' is revealed. Thus, samples S0 (without dopant or codopant) and S1 (without dopant, co-doped with AgNPs) do not show emission bands, while

S1' (without dopant, co-doped with Ag₂O) have three emission bands located at 562 nm, 598 nm and 647 nm. The mentioned bands are attributed to the presence of metallic silver in the sample. This is explained by reducing part of the silver Ag⁺ ions (present in samples due to the use of Ag₂O as a starting material) during the process of sample preparation (melting).



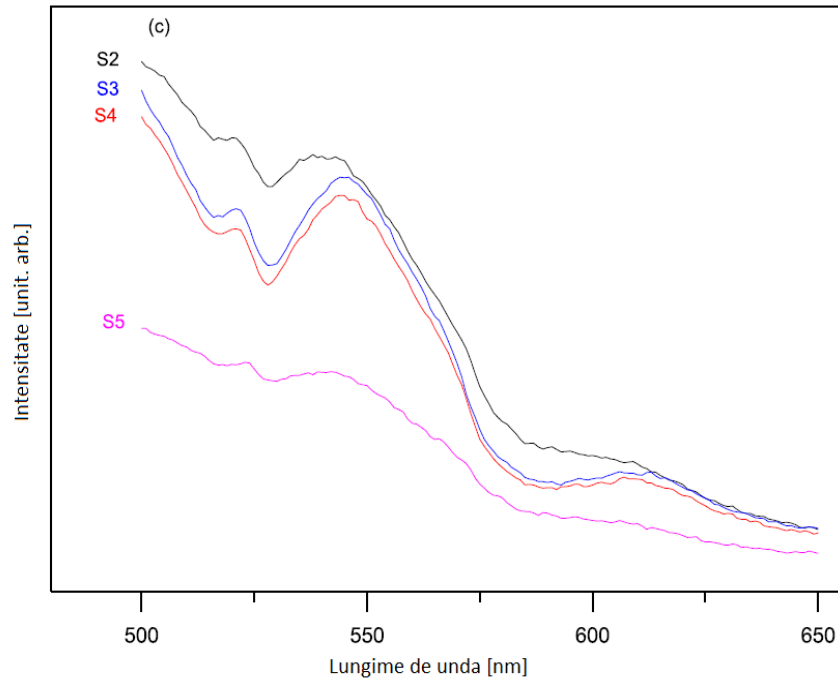


Fig. 4.20. The luminescence spectra of the samples S2, S3, S4 and S5

It can also be observed that the intensity of the emission bands from the studied samples decreases to Nd_2O_3 concentrations greater than 1% molar Nd_2O_3 . This behavior suggests that for concentrations greater than 1% molar Nd_2O_3 non-radiative mechanisms become active and a luminescence attenuation occurs.

V. CONCLUSIONS

The present paper presents data on the obtaining, structure and some properties of oxide systems based on bismuth-lead or tellurium-lead, doped with gadolinium or neodymium ions and codoped with silver ions, Ag^+ , or nanoparticles. silver, AgNPs.

The study aimed to elucidate the mechanisms by which the ion-codoping of silver or AgNPs of oxide glasses based on bismuth-lead or tellurium-lead doped with rare earth ions (Gd or Nd) produces the modification of the structure and properties of the host systems.

The systems studied were chosen due to their interesting physical properties and potential applications. Thus, these materials have i. a wide range of IR transmission, ii. each type of vitreous

lattice corresponds to several types of structural units, their interconnection being possible under certain conditions, iii. the addition of rare earth oxides greatly changes the structure and properties of the host material, etc.

The most important results obtained from the research carried out within the doctoral thesis can be summarized as follows:

1. The systems were prepared and investigated for the first time:

$(100-x-y)[\text{Bi}_2\text{O}_3 \cdot \text{PbO}] \cdot x\text{Gd}_2\text{O}_3 \cdot y\text{Ag}_2\text{O}$, $(100-x)[80\text{TeO}_2 \cdot 20\text{PbO}] \cdot 0.005\text{Ag}_2\text{O} \cdot x\text{Gd}_2\text{O}_3$,
 $(100-x)[80\text{TeO}_2 \cdot 20\text{PbO}] \cdot 0.003\text{AgNPs} \cdot x\text{Gd}_2\text{O}_3$, $80\text{TeO}_2 \cdot (19,7-x)\text{PbO} \cdot 0,3\text{AgNPs} \cdot x\text{Nd}_2\text{O}_3$ și
 $80\text{TeO}_2 \cdot (19,85-x)\text{PbO} \cdot 0,15\text{Ag}_2\text{O} \cdot x\text{Nd}_2\text{O}_3$

We mention that these glass systems are new, original, were prepared and investigated for the first time in the present study and have not been previously reported in the literature.

2. The substances used for the preparation of the studied samples were Bi_2O_3 , PbO , Gd_2O_3 , Nd_2O_3 , Ag_2O and AgNPs , respectively, of 99.5% analytical purity, in powder form. The samples obtained were glass or ceramic. Samples were prepared by melt cooling method.

3. The X-ray diffraction investigation of the samples revealed the following:

a. X-ray diffractograms of the system $(100-x-y)[\text{Bi}_2\text{O}_3 \cdot \text{PbO}] \cdot x\text{Gd}_2\text{O}_3 \cdot y\text{Ag}_2\text{O}$ showed that the samples are partially crystallized. Thus, they show the crystalline phases δ cubic Bi_2O_3 FC, simple cubic $\text{PbO}_{1.44}$, as well as traces of cubic $\text{Bi}_{1.208}\text{Gd}_{0.792}\text{O}_3$ FC. Increasing the Gd_2O_3 content reduces the sample crystallization process. No significant effect of codoping with Ag_2O was observed.

b. X-ray diffractograms of the samples $(100-x)[80\text{TeO}_2 \cdot 20\text{PbO}] \cdot 0,5\text{Ag}_2\text{O} \cdot x\text{Gd}_2\text{O}_3$ and $(100-x)[80\text{TeO}_2 \cdot 20\text{PbO}] \cdot 0,3\text{AgNPs} \cdot x\text{Gd}_2\text{O}_3$ show that the non-doped samples (without Gd_2O_3) . The crystalline phases appear after the addition of Gd_2O_3 in the samples and have been identified as $\text{Gd}_2\text{Te}_6\text{O}_{15}$, $\text{Pb}_2\text{Te}_3\text{O}_7$, namely $\text{Gd}_2\text{Te}_4\text{O}_{11}$. The amount of crystalline phases increases proportionally with the increase of gadolinium ion concentration. The size of the crystallites increases with increasing gadolinium content up to $x = 5$ mol%, then decreases, while the crystallinity of the samples increases with increasing gadolinium content throughout the composition range (faster up to $x = 5$ mol%). , then slower).

c. X-ray diffractograms of samples $80\text{TeO}_2 \cdot (19,7-x)\text{PbO} \cdot 0,3\text{AgNPs} \cdot x\text{Nd}_2\text{O}_3$ și $80\text{TeO}_2 \cdot (19,85-x)\text{PbO} \cdot 0,15\text{Ag}_2\text{O} \cdot x\text{Nd}_2\text{O}_3$ showed that non-doped samples (without Nd_2O_3) and those with low neodymium content (up to $x = 1$ mol%) are amorphous. The amorphous phase

contains clusters formed from units representing the elementary cell (approximately 44 elementary cells / cluster). For a higher content of neodymium ($x > 1\%$ mol), in addition to the amorphous phase, a crystalline phase also identified as a mixture of the crystalline phases $\text{Pb}_2\text{Te}_3\text{O}_7$ and $\text{Nd}_2\text{Te}_6\text{O}_{15}$ (for samples with $x \geq 10\%$ mol, also appears crystalline phase $\text{Nd}_2\text{Te}_4\text{O}_{11}$). The increase of the dopant concentration (Nd_2O_3) in the samples leads to an increase of the crystallization degree of the samples and the size of the crystallites, while the size of the amorphous phase clusters remains constant.

4. The investigation by IR spectrometry of the samples revealed the following:

a. In the samples from the system $(100-x-y)[\text{Bi}_2\text{O}_3 \cdot \text{PbO}] \cdot x\text{Gd}_2\text{O}_3 \cdot y\text{Ag}_2\text{O}$, the structural units BiO_3 and BiO_6 , respectively PbO_n (with $n = 3$ and 4) are present. The ratio of the quantity of structural units $\text{BiO}_6 / \text{BiO}_3$ decreases with the increase of gadolinium oxide concentration in the studied glasses.

b. In the samples from the $(100-x)[80\text{TeO}_2 \cdot 20\text{PbO}] \cdot 0,5\text{Ag}_2\text{O} \cdot x\text{Gd}_2\text{O}_3$ and $(100-x) \cdot [80\text{TeO}_2 \cdot 20\text{PbO}] \cdot 0,3\text{AgNPs} \cdot x\text{Gd}_2\text{O}_3$ units PbO_3 , PbO_4 , TeO_3 and TeO_4 are present. Based on IR data, the ratio $A_r = \text{TeO}_3 / \text{TeO}_4$ between the number of TeO_3 and TeO_4 structural units was calculated. For both series of samples, A_r decreases with increasing gadolinium content throughout the composition area. This suggests the progressive conversion of the TeO_3 structural units into TeO_4 as the content of Gd_2O_3 increases. A_r values are higher for AgNPs-codoped glass ceramic than for Ag_2O -codoped samples. This is related to the specific way in which the silver added in the host matrix is inserted in the two forms: in the case of AgNPs it is a simple insertion in interstitial positions, while in the case of Ag_2O doping, silver ions are provided which are inserted in the structural chains of the host matrix. These observations allow us to conclude that not only the content of gadolinium ions in the vitroceraamics studied, but also the nature of the codopant (Ag_2O or AgNPs) plays an important role in defining the local structure of these samples.

5. Magnetic susceptibility measurements revealed the following features common to all 3 systems studied - $(100-x-y)[\text{Bi}_2\text{O}_3 \cdot \text{PbO}] \cdot x\text{Gd}_2\text{O}_3 \cdot y\text{Ag}_2\text{O}$, $(100-x)[80\text{TeO}_2 \cdot 20\text{PbO}] \cdot 0,5\text{Ag}_2\text{O} \cdot x\text{Gd}_2\text{O}_3$ and $(100-x) [80\text{TeO}_2 \cdot 20\text{PbO}] \cdot 0,3\text{AgNPs} \cdot x\text{Gd}_2\text{O}_3$:

The magnetic behavior of the samples is due to the presence of rare earth magnetic ions, respectively Gd^{3+} and Nd^{3+} in the host matrix, bismuthed lead or tellurite lead. The values obtained for the paramagnetic Curie temperature, θ_p , suggest a Curie type behavior for the samples with low rare earth oxide content ($x < 3\%$ molar) and a Curie-Weiss type behavior for the samples with

high rare earth oxide contents. In the first case, rare earth ions are randomly distributed in the host glass matrix. In the second case, the relatively small and negative values of θ_p suggest the presence of rare earth ions as well in the form of pairs coupled through weak antiferromagnetic interactions.

6. The density measurements highlighted the following features of the investigated systems:

a. In the system $(100-x-y)[\text{Bi}_2\text{O}_3 \cdot \text{PbO}] \cdot x\text{Gd}_2\text{O}_3 \cdot y\text{Ag}_2\text{O}$, taking into account the value of the measurement errors, we can say that the compositional variation of the density shows a decrease throughout the compositional field as the concentration of ions of Gd^{3+} increases. samples. This fact, apparently contradictory (considering the higher mass of gadolinium ions than of the lattice-forming atoms, Bi and Pb), can be explained by the fact that, as shown by FTIR spectroscopy data, the addition of Gd^{3+} ions results in the conversion structural groups BiO_3 in BiO_6 , which leads to a tighter (less compact) sample structure.

b. In systems $100-x)[80\text{TeO}_2 \cdot 20\text{PbO}] \cdot 0,5\text{Ag}_2\text{O} \cdot x\text{Gd}_2\text{O}_3$ and $(100-x)[80\text{TeO}_2 \cdot 20\text{PbO}] \cdot 0,3\text{AgNPs} \cdot x\text{Gd}_2\text{O}_3$ it is found that there is a non-linear variation of the density as the content increases gadolinium of samples. Thus, for the samples co-doped with Ag_2O , an increase in density occurs with an increase in the Gd_2O_3 content up to 3 mol%, and then, for concentrations higher than Gd_2O_3 , a decrease of it follows. In the case of samples co-doped with AgNPs the density increases up to 5 mol% Gd_2O_3 , then decreases. The decrease in density is more pronounced for silver ion encoded glass ceramic. The non-linear compositional evolution of density suggests a complex mechanism of structural changes that occur in the matrix of vitroceramics studied when the gadolinium content is modified and occurs due to the role of lattice modifier played by Gd^{3+} ions, a role that is manifested by changing the ratio between the different types of structural units present in the vitroceramic lattice depending on the gadolinium content of the samples.

c. $80\text{TeO}_2 \cdot (19,7-x)\text{PbO} \cdot 0,3\text{AgNPs} \cdot x\text{Nd}_2\text{O}_3$ and $80\text{TeO}_2 \cdot (19,85-x)\text{PbO} \cdot 0,15\text{Ag}_2\text{O} \cdot x\text{Nd}_2\text{O}_3$ it is found that there is a nonlinear variation in density with increasing content of gadolinium of samples. Thus, for the system co-doped with AgNPs the density increases up to 3 mol% Nd_2O_3 after which it is kept constant. For the system co-doped with Ag_2O the density increases up to 3% molar percentage of Nd_2O_3 after which a sharp decrease occurs. We would expect that as the amount of neodymium ions increases, the heavier they are, the density will increase linearly. The nonlinear density variation according to the content of the neodymium ions highlights a more complex mechanism that involves the $\text{TeO}_3 \rightarrow \text{TeO}_4$ conversion process of the

structural units determined by the increase of the neodymium ion content. Thus for low dopant concentrations ($\leq 3\%$ mol Nd_2O_3), heavy neodymium ions are inserted into the host matrix without involving structural changes, leading to an increase in sample density. For high concentrations ($> 3\%$ mol Nd_2O_3), the neodymium ions play the role of lattice modifiers, generating the conversion of TeO_3 structural units into TeO_4 structural units, which leads to a tighter (less compact) structure, respectively to a decrease of density. Increasing the Nd_2O_3 content above 3% mol results in an increase in the number of non-bridging oxygen atoms, confirmed by FTIR spectroscopy data.

7. The UV-Vis spectrometry study of the samples revealed the following features of the investigated systems:

a. In $80\text{TeO}_2 \cdot (19,7-x)\text{PbO} \cdot x\text{Nd}_2\text{O}_3 \cdot 0,3\text{AgNPs}$ and $80\text{TeO}_2 \cdot (19,85-x)\text{PbO} \cdot x\text{Nd}_2\text{O}_3 \cdot 0,15\text{Ag}_2\text{O}$ systems, it is found that the samples that do not contain neodymium have no absorption peaks. The other samples show eight peaks corresponding to the transitions from the fundamental level $^4\text{I}_{9/2}$ to various excited levels of Nd^{3+} ions ($^4\text{I}_{9/2} \rightarrow ^4\text{G}_{9/2}, ^4\text{G}_{7/2}, ^4\text{G}_{5/2}, 2\text{H}_{11/2}, ^4\text{F}_{9/2}, ^4\text{S}_{3/2} + ^4\text{F}_{7/2}, ^4\text{F}_{5/2}, ^4\text{F}_{3/2}$). Increasing the concentration of dopant (neodymium) in samples only changes the intensity of the peaks, increasing it, not their location (with minor exceptions). The values calculated for the non-fallauxetic parameter (β) and for the binding parameter (δ) showed that in the vitroc ceramic systems studied, the bonds of Nd^{3+} -ligand are ionic.

b. The gap energy, E_g , of the samples in the $80\text{TeO}_2 \cdot (19,7-x)\text{PbO} \cdot x\text{Nd}_2\text{O}_3 \cdot 0,3\text{AgNPs}$ și $80\text{TeO}_2 \cdot (19,85-x)\text{PbO} \cdot x\text{Nd}_2\text{O}_3 \cdot 0,15\text{Ag}_2\text{O}$ systems shows a nonlinear variation with neodymium content of samples. The highest values of E_g were determined for samples S2 (doped with 1% mol Nd_2O_3 and co-doped with AgNPs) and S4 (doped with 5% mol Nd_2O_3 and co-doped with Ag_2O). For concentrations greater than 5% mol, E_g shows a sharp decrease, probably due to the increase in the amount of unbound oxygen.

8. The luminescence spectrometry study of $80\text{TeO}_2 \cdot (19,7-x)\text{PbO} \cdot x\text{Nd}_2\text{O}_3 \cdot 0,3\text{AgNPs}$ and $80\text{TeO}_2 \cdot (19,85-x)\text{PbO} \cdot x\text{Nd}_2\text{O}_3 \cdot 0,15\text{Ag}_2\text{O}$ systems revealed the following features of these systems:

a. Samples without dopant and codopant (S0) and without dopant, co-doped with AgNPs (S1) do not produce emission peaks, while the sample without dopant, co-doped with Ag_2O (S1') shows three emission peaks located at 562 nm, 598 nm and 647 nm. The mentioned peaks are attributed to the presence of metallic silver in the sample. This is explained by the reduction of some of the silver ions Ag^+ (present in samples due to the use of Ag_2O as a starting material) to

Ag⁰ (metallic silver) during the process of sample preparation (melting), as a result of the relatively high melting temperature. Metallic silver atoms can form clusters or even silver nanoparticles.

b. The irradiation of the samples with an excitation radiation with the wavelength of 808 nm produces the excitation of AgNPs by the TPA (two-photon absorption) mechanism at the same level of excitation as would be obtained by the direct excitation with a 400 nm wave. When a silver metal nanoparticle thus excited is very close to an Ag⁺ ion (or similar luminescence center), the luminescence emission occurs.

c. The luminescence spectra of the neodymium doped samples have 4 emission bands located at 521, 542, 560 and 608 nm and which have been assigned as follows:

- the 521 nm band is assigned to the f-f transitions of the Nd³⁺ ions from the level ²P_{1/2} to ⁴I_{13/2}.

- The 542 nm band is due to the transition from the ⁴G_{7/2} excited level to the basic ⁴I_{9/2} level.

- The 560 nm band is due to the presence of AgNPs near another luminescent center of the sample.

- the band from 608 nm is assigned to the transition from the excited level ⁴G_{7/2} to the level of ⁴I_{11/2} and from the excited level ⁴G_{5/2} + ²G_{7/2} to the fundamental level ⁴I_{9/2} of the Nd³⁺ ions [29, 30, 39].

d. The intensity of the emission bands decreases at concentrations of Nd₂O₃ greater than 1% molar Nd₂O₃. This behavior suggests that for concentrations greater than 1% molar Nd₂O₃ non-radiative mechanisms become active and a luminescence attenuation occurs.